Korean J. Chem. Eng., 38(7), 1381-1393 (2021)
DOI: 10.1007/s11814-021-0793-5

pISSN: 0256-1115
eISSN: 1975-7220

Template-assisted preparation of metal-modified SAPO-34 molecular sieves for the catalysis of methanol-to-olefins

Jihui Yao*, Jiapeng Jiao*, Ruiqiang Liu*, Fei Zha*,†, Xiaojun Guo*, Xiaohua Tang*, Haifeng Tian*, and Yue Chang*,**

*College of Chemistry & Chemical Engineering, Northwest Normal University, Lanzhou 730070, Gansu, China
**Key Laboratory of Eco-functional Polymer Materials of the Ministry of Education, Lanzhou 730070, Gansu, China
(*Received 15 December 2020 • Revised 11 March 2021 • Accepted 28 March 2021*)

Abstract−To improve the dispersion of metals and to enhance the catalytic performance of SAPO-34 molecular sieves, the template-assisted method was applied to synthesize Co, Ni and Zn modified SAPO-34 molecular sieves by using palygorskite as silicon source and tetraethylammonium hydroxide as template. The metal modified SAPO-34 molecular sieves were characterized by XRD, SEM, XPS, N_2-adsorption-desorption, NH_3-TPD, FTIR, ICP-AES and TG. The N atoms of tetraethylammonium hydroxide exhibited the different forces to three metal ions, thus the acidity of the molecular sieves was further regulated. Compared with metal modified SAPO-34 molecular sieves prepared by impregnation, metal modified SAPO-34 molecular sieves prepared by template-assisted maintained higher surface area, bigger pore volume and better dispersion of metals. The catalytic performance of metal modified SAPO-34 molecular sieves prepared by template-assisted method in the reaction of methanol-to-olefins (MTO) was investigated in the fixed bed reactor. Under the reaction conditions that the reaction temperature was 400 °C, the reaction pressure was 0.1 MPa, the feed WHSV was 2.0 h^{-1} and the mass of catalyst was 0.5 g, Ni modified SAPO-34 molecular sieves exhibited great methanol conversion and high selectivity to light olefins. The selectivity of light olefins reached 95.7%.

Keywords: SAPO-34 Molecular Sieves, Metal Modification, Palygorskite, MTO, Template-assisted, Light Olefins

INTRODUCTION

Light olefins, including ethylene, propylene and butylene, are significantly fundamental chemical raw materials that are mainly obtained from naphtha steam cracking and fluid catalytic cracking processes, which severely depend on petroleum [1]. Methanol-to-olefin (MTO), as an alternative route for obtaining light olefins from abundant non-petroleum resources such as natural gas, coal, biomass and solid wastes, has attached great attention in the recent years [2-5]. With the chabazite cages (0.67×0.67×1 nm), small 8-ring pore openings (0.38×0.38 nm), moderate acidity and high hydrothermal stability, SAPO-34 molecular sieves have been proven to have excellent catalysis performance in MTO reaction [6-10]. However, its microporous structure and relatively large crystals usually cause coke deposition, making serious diffusion limitation and resulting in rapid deactivation [11-13].

To this day, numerous tactics, such as decorating the acidity, optimizing the synthesis procedure, adjusting the crystal size and introducing hierarchical structures into the molecular sieves, have been employed to develop the catalytic performance of SAPO-34 molecular sieves in MTO [2,4,6,14-16]. In particular, metal modified SAPO-34 molecular sieves have attracted great attention. The metal oxides occupy partially Brønsted acid sites to control the acid amount and strength of molecular sieves [2,17-19]. However, by using methods mentioned to decorate structure and acidity of molecular sieves may cause two inevitable issues: the micropores (<2 nm) of molecular sieve framework can be blocked by the metal nanoparticles with diameters ranging from 1.5 to 4 nm, and the metal nanoparticles are just attached on the exterior surface, which results in unsatisfactory catalytic performance [20]. Hence, developing a novel synthesis approach to obtain higher dispersity of metal in molecular sieves for achieving high performance in MTO reaction would be a promising route. Lately, the one-pot synthesis of Cu-SAPO-34, using Cu-amine complex or a combination of Cu-amine complex with traditional organic structure directing agents (OSDAs) as template, has the merits of better metal dispersion, easy regulation of metal loading and simplicity in entire synthesis steps [21-24].

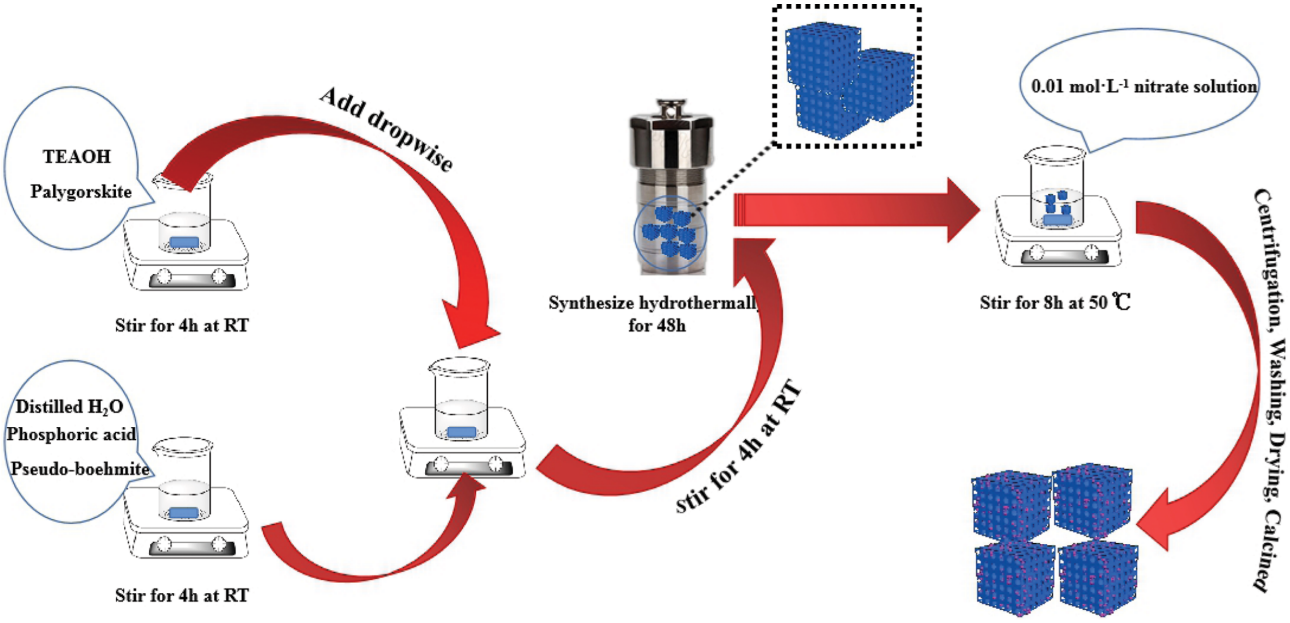
In our present work, Co, Ni and Zn were introduced into SAPO-34 molecular sieves using acidified palygorskite as silicon source with straightforward template-assisted method. The relationship between metals and the template was studied. The catalytic performance of metal modified SAPO-34 molecular sieves was evaluated in the MTO reaction.

EXPERIMENTAL

1. Chemicals and Materials

$Zn(NO_3)_2{\cdot}6H_2O$, $Ni(NO_3)_2{\cdot}6H_2O$, $Co(NO_3)_2{\cdot}6H_2O$, phosphoric acid (85 wt%) and tetraethylammonium hydroxide (TEAOH) were all of the analytical grade and were purchased from Macklin Co. LTD. Palygorskite, Pseudo-boehmite (Al_2O_3, 70 wt%) and hydrogen

†To whom correspondence should be addressed.
E-mail: zhafei@nwnu.edu.cn
Copyright by The Korean Institute of Chemical Engineers.



Scheme 1. Synthesis procedure of metal modified SAPO-34 molecular sieves prepared by template-assisted method.

chloride (36-38 wt%) were all of the industrial grade. Distilled water was used in all experiments.

2. Preparation of Metal-modified SAPO-34

2-1. Template-assisted Approach

The preparation of SAPO-34 molecular sieves with the organic structure directing agent (OSDA) of tetraethylammonium hydroxide (TEAOH) and acidified palygorskite was carried out according to our previous work [25]. In the current work, the mixture of as-made SAPO-34 molecular sieves without pre-removing template in 0.01 mol·L^{-1} nitrate solution of Co, Ni and Zn with a liquid-to-solid ratio of 30 ml·g^{-1} was stirred at 50 °C for 8.0 h, respectively. After undergoing centrifuging, washing and drying, the obtained powder was calcined at 550 °C for 8.0 h to remove the organic template. The obtained metal modified SAPO-34 molecular sieves were denoted as Co-SAPO-34-8h, Ni-SAPO-34-8h and Zn-SAPO-34-8h, respectively. The synthesis procedure is schematically depicted in Scheme 1.

2-2. Impregnation Approach

To compare with Co-SAPO-34-8h, Ni-SAPO-34-8h and Zn-SAPO-34-8h molecular sieves prepared by template-assisted method, SAPO-34 molecular sieves were prepared by the impregnation method. 1.0 g of calcined SAPO-34 molecular sieves was impregnated in the solution containing 1.1 g of distilled water and a certain amount of metal nitrate, then aged at 50 °C for 8.0 h. The subsequent processes were similar to the template-assisted approach. The prepared metal modified SAPO-34 molecular sieves were named as Co-SAPO-34-im, Ni-SAPO-34-im and Zn-SAPO-34-im, separately.

3. Catalyst Characterization

The powder X-ray diffraction patterns (XRD) of samples were detected on the Rigaku D/Max-2400 X-ray diffractometer (λ=1.5406 Å) with a Cu K_α radiation source. The operation conditions were 40 KV and 60 mA in a 2θ ranging from 5° to 80°. The lattice parameter and crystallinity were obtained by MDI Jade (version of 6.0). The morphology of the samples was observed on the ULTRA plus scanning electron microscope (SEM) equipped with a Noran System Six energy dispersive spectroscopy (EDS) system. The X-ray photoelectron spectroscopy (XPS) measurement was carried out on the Thermo ESCALAB 250XI X-ray photoelectron spectrometer with a monochromated Al K_α radiation source (150 W, hv= 1,486.6 eV). The binding energy was calibrated by adventitious carbon deposit C(1s) with Eb=284.8 eV. Nitrogen adsorption-desorption technique was used to analyze the Brunauer-Emmett-Teller (BET) surface area, pore volume and pore size of samples by using the Quantachrome Autosorb-1 apparatus. The pore volume was determined at a relative pressure (P/P_o) of 0.99. Fourier transform infrared (FT-IR) spectra were examined by the Digilab-FTS3000 photometer. Prior to testing, the samples were dried at 100 °C overnight and then mechanically mixed with KBr at a mass ratio of 1 : 100. NH_3 temperature-programmed desorption (NH_3-TPD) of samples were carried out on the Betterwork MFTP3060 multifunction catalyst analysis system (Xiamen, China). Thermogravimetric (TG) analysis was implemented on the Perkin-Elmer TG/DTA-6300 analyzer in the presence of the flowing air at a heating rate of 5 °C·min^{-1} from room temperature to 800 °C. Elemental analysis for Co, Ni and Zn of calcined samples was obtained by inductively coupled plasma atomic emission spectrometry (ICP-AES, Agilent 5110.) after dissolving the samples into 1 mol·L^{-1} HNO_3 solution.

4. Catalytic Reaction Tests

The activity of catalysts in the MTO reaction was evaluated at 400 °C in a stainless-steel fix-bed reactor. Prior to the test, 0.5 g of catalyst was activated in a pure N_2 (20 ml·min^{-1}) at 400 °C for 1 h. Then the methanol of 0.02 ml·min^{-1} was feed into the reactor with a N_2 flowing of 20 ml·min^{-1}. The online gas chromatography (GC2060, Shanghairuimin, China) was utilized to detect products,

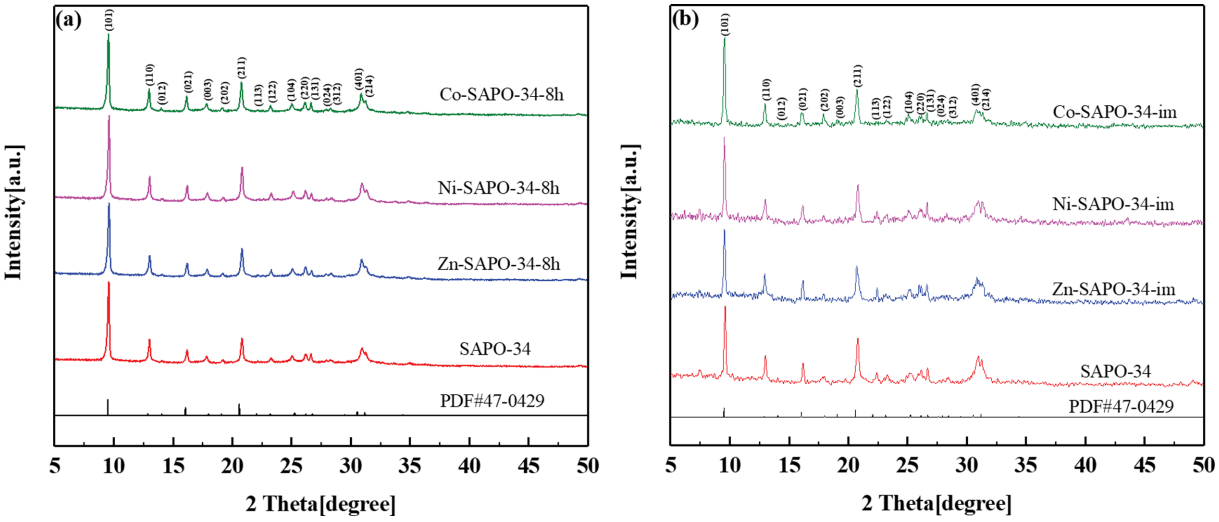


Fig. 1. XRD patterns of (a): Co-SAPO-34-8h, Ni-SAPO-34-8h, Zn-SAPO-34-8h and SAPO-34, (b): Co-SAPO-34-im, Ni-SAPO-34-im, Zn-SAPO-34-im and SAPO-34.

Table 1. Lattice parameters, element content and relative crystallinity of samples

Samples	Lattice parameters[a] (Å)			Element content[b] (%)	Relative crystallinity[c] (%)
	a	b	c		
SAPO-34	13.68	13.68	15.00	-	100
Co-SAPO-34-im	13.81	13.81	14.70	1.76	97.50
Ni-SAPO-34-im	13.67	13.67	15.02	1.75	97.60
Zn-SAPO-34-im	13.66	13.66	14.99	1.78	97.57
Co-SAPO-34-8h	13.67	13.67	14.96	0.24	96.79
Ni-SAPO-34-8h	13.64	13.64	14.90	0.28	96.82
Zn-SAPO-34-8h	13.61	13.61	14.87	0.50	96.53

[a]The lattice parameters were precisely revised by Jade 6.0.
[b]The element content was determined by ICP-AES.
[c]Relative crystallinity= $\frac{\text{crystallinity (modified SAPO-34)}}{\text{crystallinity (SAPO-34)}} \times 100\%$.

equipped with a thermal conductivity detector (TCD) and a capillary column (CB-PLOT Q Al_2O_3/M) to separate the products. The selectivity of light olefins was calculated by the area normalization method.

RESULTS AND DISCUSSION

1. Characterization

1-1. X-ray Diffraction (XRD) Analysis

The XRD patterns of the catalysts are portrayed in Fig. 1. The typical CHA structure was detected for all catalysts and no amorphous phase was discovered [4]. The characteristic peaks of catalysts at 2θ=9.54°, 12.97°, 14.02°, 16.08°, 17.68°, 19.07°, 20.71°, 22.05°, 23.17°, 25.12°, 26.12°, 26.704°, 27.93°, 28.45°, 30.81° and 31.27° are consistent with the standard card of PDF#47-0429 (SAPO-34). The characteristic peaks of metal oxides were not discovered due to the high dispersion and low content of metals [21]. In addition, the lattice parameters and relative crystallinity of molecular sieves were further employed to investigate the impact of metal introduced into molecular sieves on crystal framework, as shown in Table 1. Lattice parameters (a, b and c) refer to the arris length of each parallel hexahedron unit, which are the important basic parameters of the crystal structure. It could be found clearly that little change was outcropped in the lattice parameters for all catalysts, indicating that the introduction of metal species made obvious difference to the framework of SAPO-34 molecular sieves. The element content of Co, Ni and Zn was 0.24%, 0.28% and 0.50% for Co-SAPO-34-8h, Ni-SAPO-34-8h and Zn-SAPO-34-8h, respectively, indicating that the N atoms of TEAOH have different forces to Co^{2+}, Ni^{2+} and Zn^{2+}. Moreover, a slight change in relative crystallinity for metal modified SAPO-34 molecular sieves prepared by template-assisted was discovered, indicating that framework of as-made SAPO-34 molecular sieves may be adversely impacted by long time water treatment.

1-2. Scanning Electron Microscope (SEM) and Elemental (EDS) Analysis

SEM and metallic EDS images of SAPO-34 molecular sieves are displayed in Fig. 2. All the samples mainly exhibit a cubic like

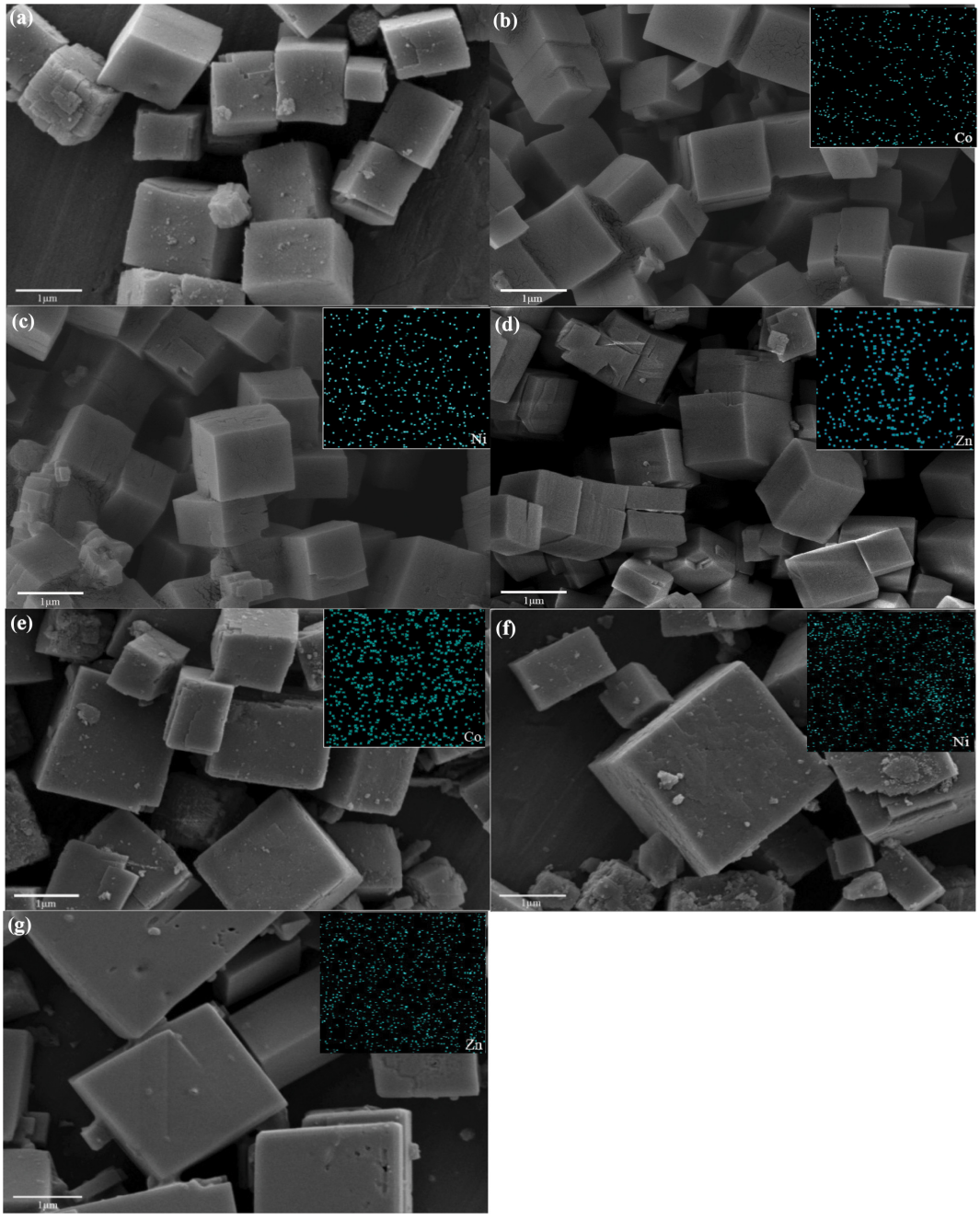


Fig. 2. SEM and EDS images of (a): SAPO-34, (b): Co-SAPO-34-8h, (c): Ni-SAPO-34-8h, (d): Zn-SAPO-34-8h, (e): Co-SAPO-34-im, (f): Ni-SAPO-34-im and (g): Zn-SAPO-34-im.

morphology, with a change in the crystalline size ranging from 1.0 to 3.0 μm [26]. Surprisingly, the shape of Co-SAPO-34-8h, Ni-SAPO-34-8h and Zn-SAPO-34-8h was not seriously undermined during the post-processing. It can be seen from the EDS images that although metal content in metal modified SAPO-34 molecular sieves prepared by template-assisted method is lower than that of metal modified SAPO-34 molecular sieves prepared by impregnation, metal species are well dispersed. The ionic radius of Co, Ni and Zn is 61 pm, 70 pm and 75 pm, respectively. Thus, a part of metal ions can enter into the cages and channels of as-made SAPO-34 molecular sieves by interaction with N atoms of TEAOH. Meanwhile, metal ions are attached to the surface of SAPO-34 molecular sieves due to the microporosity of molecular sieves. This means that the N atoms from TEAOH as anchoring sites can control the dispersion of metal species well.

1-3. X-ray Photoelectron Spectroscopy (XPS) Analysis

XPS was employed to investigate the interplay between N atoms of TEAOH and metal cations (Co^{2+}, Ni^{2+} and Zn^{2+}) based on the binding energy shift of N 1*s*, Co $2p_{3/2}$, Ni $2p_{3/2}$ and Zn $2p_{3/2}$ as depicted in Fig. 3. The binding energy of N 1*s* for as-made Co-SAPO-34, Ni-SAPO-34 and Zn-SAPO-34 slightly outpace that of as-made SAPO-34, illustrating that the charges of N atoms of TEAOH

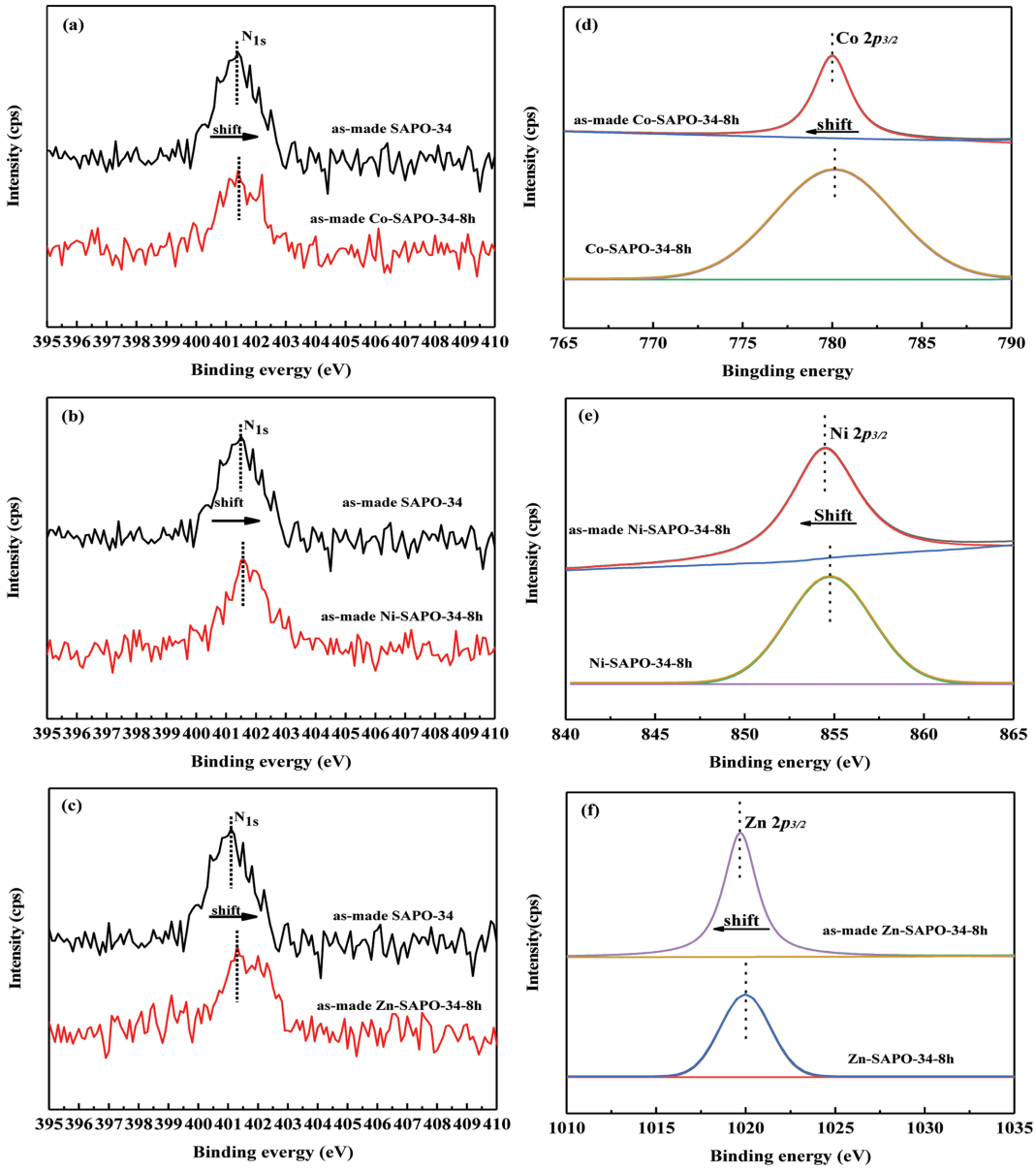


Fig. 3. XPS central location spectra of N 1s of (a): as-made SAPO-34, as-made Co-SAPO-34-8h, (b): as-made SAPO-34, as-made Ni-SAPO-34-8h, (c): as-made SAPO-34, as-made Zn-SAPO-34-8h, and M 2p3/2 (M=Co, Ni and Zn) of (d): as-made Co-SAPO-34-8h, Co-SAPO-34-8h, (e): as-made Ni-SAPO-34-8h, Ni-SAPO-34-8h, (f): as-made Zn-SAPO-34-8h, Zn-SAPO-34-8h.

are transferred to the metal cations as shown in Fig. 3(a)-(c). Likewise, the binding energy of $2p_{3/2}$ for Co-SAPO-34-8h, Ni-SAPO-34-8h and Zn-SAPO-34-8h slightly surpass that of as-made Co-SAPO-34-8h, Ni-SAPO-34-8h and Zn-SAPO-34-8h, revealing that the electron density around metal cations increases due to electron transfer between N atoms of TEAOH and metal cations as depicted in Fig. 3(d)-(f). Hence, the N atoms of TEAOH are the anchoring sites for Co^{2+}, Ni^{2+} and Zn^{2+}, which is congruent with literature reported [22,27,28]. In addition, the different shifts in the samples of Co-SAPO-34-8h, Ni-SAPO-34-8h and Zn-SAPO-34-8h are observed in the spectra of N 1*s*. Meanwhile, it can be apparently observed that the gap of binding energy of Zn-SAPO-34-8h at $2p_{3/2}$ is larger than that of others, showing that N atoms of TEAOH exist stronger interaction with Zn cations, leading to the introduction of large amount of Zn cations into SAPO-34 molecular sieves, which is in accordance with the data detected from ICP-AES. In summary, N atoms of TEAOH as an anchoring sites can reasonably regulate the metal content in SAPO-34 molecular sieves.

XPS was further carried out to determine the chemical state of metal species, as shown in Fig. 4. The detailed data based on full spectra are listed in Table 2. The binding energy located at 24.1 eV, 72.8 eV, 98.2 eV, 116.8 eV, 133.2 eV, 149.4 eV, 165.5 eV, 188.8 eV, 281.8 eV and 527.7 eV is assigned to the O 2*s*, Al 2*p*, Si 2*p*, Al 2*s*, P 2*p*, Si 2*s*, P 2*s*, C 1*s* and O 1*s*, respectively. The binding energy of $2p_{3/2}$ central located in 780.1 eV, 854.8 eV, 1,019.7 eV and $2p_{1/2}$ central location at 795.9 eV, 875.6 eV, 1,042.8 eV are assigned to the

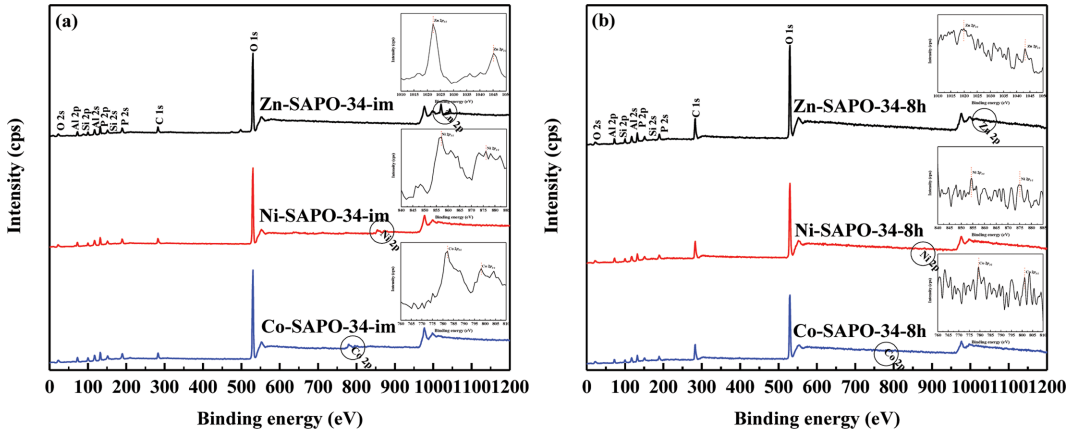


Fig. 4. XPS central location spectra of (a): Co-SAPO-34-im, Ni-SAPO-34-im, Zn-SAPO-34-im, (b): Co-SAPO-34-8h, Ni-SAPO-34-8h, Zn-SAPO-34-8h.

Table 2. Central location of binding energy of samples

Samples	Central location of binding energy[a]														
	O2*s*	Al2*p*	Si2*p*	Al2*s*	P2*p*	Si2*s*	P2*s*	C1*s*	O1*s*	Co2*P*		Ni2*P*		Zn2*P*	
										$2P_{3/2}$	$2P_{1/2}$	$2P_{3/2}$	$2P_{1/2}$	$2P_{3/2}$	$2P_{1/2}$
Co-SAPO-34-im	24.1	72.7	98.2	116.8	130.8	149.3	188.8	281.8	527.7	780.1	795.8	-	-	-	-
Ni-SAPO-34-im	24.1	72.7	98.2	116.8	130.8	149.3	188.8	281.8	527.7	-	-	854.8	875.3	-	-
Zn-SAPO-34-im	24.1	72.7	98.2	116.8	130.8	149.3	188.8	281.8	527.7	-	-	-	-	1,019.8	1,412.8
Co-SAPO-34-8h	24.0	72.8	98.2	116.8	130.8	149.4	188.8	281.8	527.7	780.1	795.9	-	-	-	-
Ni-SAPO-34-8h	23.8	72.7	98.1	116.8	130.8	149.4	188.8	281.8	527.7	-	-	854.8	875.4	-	-
Zn-SAPO-34-8h	24.0	72.7	98.2	116.8	130.7	149.4	188.8	281.8	527.6	-	-	-	-	1,019.7	1,042.8

[a]The central location of binding energy was calculated by XPS.

Table 3. Surface area, pore volume and pore size of samples

Samples	Surface area ($m^2 \cdot g^{-1}$)			Pore volume[a] ($cm^3 \cdot g^{-1}$)			Pore size[b] (nm)
	S_{total}	S_{micro}	S_{ext}	V_{total}	V_{micro}	V_{meso}	
SAPO-34	539.20	513.81	25.39	0.28	0.24	0.04	2.06
Co-SAPO-34-im	489.73	464.27	25.45	0.25	0.22	0.03	2.17
Ni-SAPO-34-im	482.69	454.08	28.61	0.24	0.21	0.03	2.19
Zn-SAPO-34-im	471.39	451.01	20.38	0.24	0.21	0.03	2.17
Co-SAPO-34-8h	541.53	507.60	33.93	0.30	0.24	0.06	2.20
Ni-SAPO-34-8h	539.58	505.46	34.12	0.30	0.24	0.06	2.20
Zn-SAPO-34-8h	547.39	515.14	32.25	0.30	0.24	0.06	2.23

[a]The data of pore volume were obtained by the BJH method.
[b]The data of pore size were calculated by the BJH method.

metal oxide corresponding to Co, Ni and Zn, respectively. The $2p_{3/2}$ and $2p_{1/2}$ peaks of metal species in the molecular sieves are narrow and symmetric, showing that metal species in molecular sieves present at a single chemical state [29]. In addition, as the higher electronegativity of the lattice oxygen of the molecular sieves is relative to O^{2-} ligand, the binding energy located at lower region is reasonably allocated to the coordination between metal cations and lattice oxygen of the molecular sieves [22,30].

1-4. Specific Surface Area (BET) Analysis

Nitrogen adsorption-desorption isotherms of all SAPO-34 molecular sieves are displayed in Fig. 5. All the samples exhibit a typical type-IV isotherm with the H_4 type hysteresis loops [31]. The isotherms have sharp uptake in the region of $P/P^0<0.2$, demonstrating that SAPO-34 molecular sieves exist as micropore structure [32]. The obviously appearing H_4 type hysteresis loops at relative pressure ranging from 0.4 to 0.9 indicate the existence of mesopores structure [33]. In addition, the variation trend of pore size distribution further proves the presence of mesopore structure in SAPO-34 molecular sieves. Based on the detailed data of SAPO-34 molecular sieves calculated from the nitrogen adsorption-desorp-

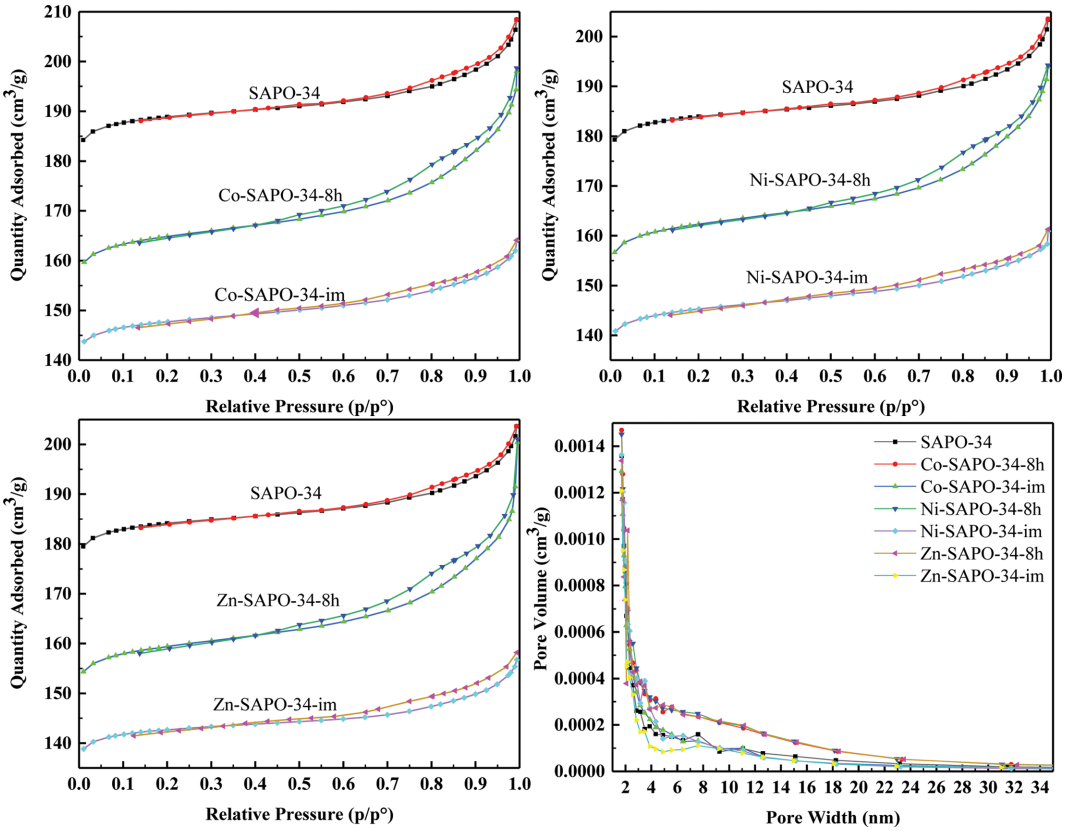


Fig. 5. Nitrogen adsorption-desorption isotherms and pore size distribution curve of the samples.

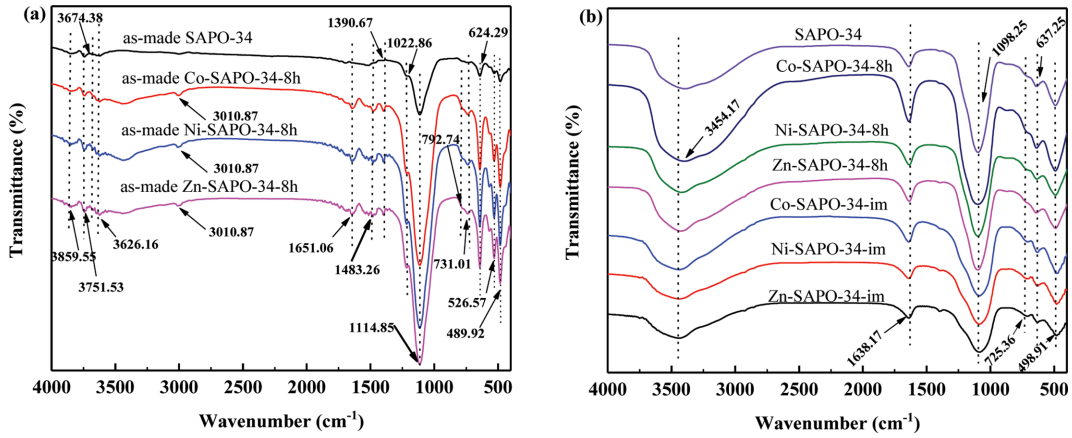


Fig. 6. FT-IR spectra of (a): as-made SAPO-34 and (b): calcined SAPO-34.

tion isotherms, as shown in Table 3; all SAPO-34 molecular sieves possess high BET and micropore surface area, high pore volume, and the average pore size is approximate to 2.20 nm. Compared to the SAPO-34 molecular sieves, the surface area and pore volume of metal modified SAPO-34 molecular sieves prepared by impregnation decrease obviously, showing that the pore channels of SAPO-34 molecular sieves are blocked partially by metal species. Also, this means that the diffusion limitation of products will be enhanced for metal modified SAPO-34 molecular sieves prepared by impregnation. On the contrary, the surface area and pore volume of metal modified SAPO-34 molecular sieves prepared by template-assisted method remain unchanged, illuminating that metal species may be highly dispersed in SAPO-34 molecular sieves [22]. Moreover, a slight increase of mesopore volume and pore size is observed in Co-SAPO-34-8h, Ni-SAPO-34-8h and Zn-SAPO-34-8h.

1-5. Infrared (FT-IR) Analysis

The Fourier transformation infrared (FTIR) spectra were utilized to further investigate the surface groups of the catalysts as shown in Fig. 6. In the as-made SAPO-34, the adsorption peaks at 1,390.67 cm^{-1} and 1,483.26 cm^{-1} are associated with the vibration of C-H bond,

which corresponds to the -CH_3 and -CH_2- species derived from TEAOH, respectively. The adsorption peaks located at 1,651.06 cm^{-1} and 3,010.87 cm^{-1} are considered as the vibration and stretching vibration of N-H band of TEAOH. The adsorption peak located at 1,022.86 cm^{-1} is attributed to the vibration of C-N band of TEAOH. The vibrations of Si species, consisting of T-O bending of silicon tetrahedra, T-O bending in 6-membered rings, symmetric stretching and asymmetric stretching of T-O-T, are detected at 489.92 cm^{-1}, 624.26 cm^{-1} and 731.01 cm^{-1}, respectively. Moreover, the vibration of hydroxyl at 3,626.16 cm^{-1}, 3,674.38 cm^{-1}, 3,751.53 cm^{-1} and 3,859.55 cm^{-1} correspond to Si-OH-Al, Si-OH, P-OH and Al-OH, respectively. Both of the fresh peaks at 526.57 cm^{-1} and 792.74 cm^{-1} are discovered, which may be ascribed to the coordination of N atoms of TEAOH with metal ions. In calcined SAPO-34, the vibrations at 499 cm^{-1}, 637 cm^{-1}, 725 cm^{-1} and 1,098 cm^{-1} are assigned to the T-O bending of silicon tetrahedra, T-O bending in 6-membered rings, T-O-T symmetric stretching and asymmetric stretching of TO_4 tetrahedra, respectively [34]. The absorption peak at 1,638 cm^{-1} is regarded as hydroxyl vibration of water absorbed on molecular sieves [3]. In addition, the adsorption band surrounded at about 3,400 cm^{-1} is attributed to bridging hydroxyl (Si-OH-Al) groups pointing towards the center of the elliptical cages [4]. This is a genre of Si-OH-Al group related to the active sites for acid-catalyzed reaction [3].

1-6. Ammonia Temperature-programmed Desorption (NH_3-TPD) Analysis

The acid strength and the number of total acid sites of the catalysts were evaluated by NH_3-TPD technique as shown in Fig. 7. For all samples, there are two peaks at 140-280 °C and 330-480 °C. The weak and strong acid sites are relevant to low and high-temperature desorption peaks, respectively. The two peaks of the catalysts in the NH_3-TPD profiles are deconvoluted into the three peaks by Gaussian peak deconvolution method and are denoted as α, β and γ peak, respectively. The α peak is assigned to the weak acid sites corresponding to hydroxyl groups (such as P-OH, Si-OH and Al-OH), which hardly show any catalytic active for MTO reaction [4]. The β and γ peaks are separately attributed to the moderate and strong acid sites matched to Brønsted acid sites (Si-OH-Al), which generally has been known as the active sites for MTO reaction [35]. The peaks of weak and strong acid sites in metal modified SAPO-34 molecular sieves prepared by template-assisted method have a slight shift to low temperature by comparison with SAPO-34 molecular sieves, showing that the strength of acid sites of molecular sieves can be regulated by the interaction between N atoms in the TEAOH and metal ions. In addition, the peaks of weak and strong acid sites in metal modified SAPO-34 molecular sieves prepared by impregnation move to lower temperature than that of metal modified SAPO-34 molecular sieves prepared by

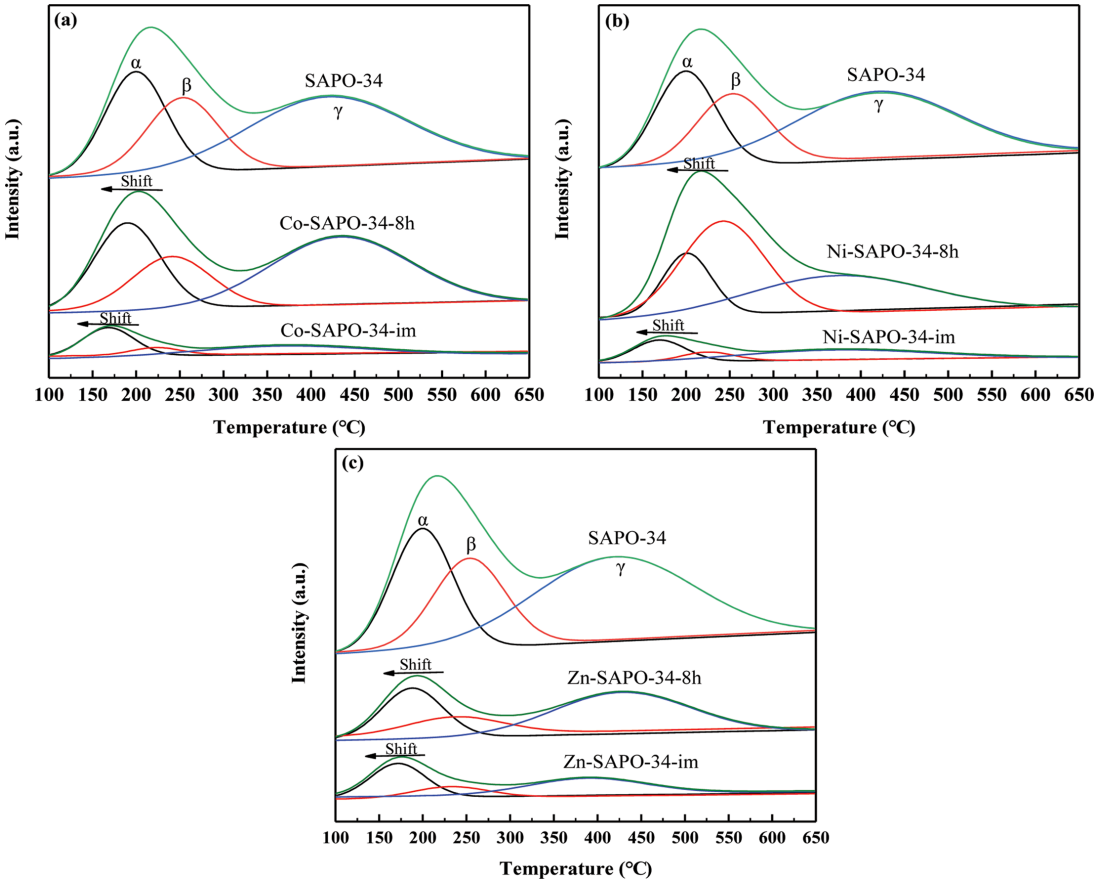


Fig. 7. NH_3-TPD profiles of (a): SAPO-34, Co-SAPO-34-8h, Co-SAPO-34-im, (b): SAPO-34, Ni-SAPO-34-8h, Ni-SAPO-34-im, (c): SAPO-34, Zn-SAPO-34-8h, Zn-SAPO-34-im.

Table 4. Acidity and coke deposition rate of samples

Samples	Acidity[a] (NH_3 absorption ($mmol \cdot g^{-1}$))					Coke deposition rate[b] ($mg \cdot h^{-1}$)
	α	β	γ	$\beta+\gamma$	$\alpha+\beta+\gamma$	
SAPO-34	11.25	9.32	18.10	27.42	38.67	0.10
Co-SAPO-34-im	2.47	0.61	3.09	3.70	6.17	0.18
Ni-SAPO-34-im	2.75	1.09	2.62	3.71	6.46	0.16
Zn-SAPO-34-im	2.10	0.80	3.86	4.66	6.76	0.17
Co-SAPO-34-8h	9.57	6.85	16.67	23.52	33.09	0.09
Ni-SAPO-34-8h	5.44	14.32	12.60	26.92	32.36	0.09
Zn-SAPO-34-8h	4.32	2.36	8.22	10.58	14.90	0.08

[a]The amount of acid sites were calculated from NH_3-TPD results.
[b]The rate of coke deposition was obtained by TG.

Table 5. Catalytic performance and lifetime of catalysts

Samples	Products selectivity (%)						Catalytic lifetime (min)
	CH_4	C_2^0-$C_4^{0②}$	$C_2^=$	$C_3^=$	$C_4^=$	$C_2^=$-$C_4^{=①}$	
SAPO-34	3.39	4.58	28.93	51.58	9.92	92.03	300
Co-SAPO-34-im	3.52	7.63	35.11	41.55	12.19	88.85	210
Ni-SAPO-34-im	3.92	6.12	34.10	44.09	11.76	89.94	240
Zn-SAPO-34-im	3.20	8.09	39.61	42.92	6.182	88.71	210
Co-SAPO-34-8h	2.98	2.16	28.27	52.99	13.60	94.86	330
Ni-SAPO-34-8h	2.81	1.48	27.57	52.82	15.32	95.71	360
Zn-SAPO-34-8h	3.48	5.20	28.45	49.01	13.85	91.31	300

①: $C_2^=$-$C_4^=$: C_2-C_4 olefins; ②: C_2^0-C_4^0: C_2-C_4 alkane. Reaction conditions: T=400 °C, WHSV=2.0 h^{-1}.

template-assisted method, indicating the strength of acid sites is weakened strongly. As is evident from the data in Table 4, the amount of total acid sites for metal modified SAPO-34 molecular sieves prepared by template-assisted method, except for Zn-SAPO-34-8h, slightly decreases in comparison with SAPO-34 molecular sieves. The amount of total acid sites for metal modified SAPO-34 molecular sieves prepared by impregnation is lower than that of metal modified SAPO-34 molecular sieves prepared by template-assisted method. This means that the introduction of massive metal into SAPO-34 molecular sieves prepared by impregnation will cause a dramatic decrease of the number of total acid sites. It was considered that the insufficient amount of total acid sites could result in incomplete methanol conversion [4]. Moreover, the proportion of weak-acid sites is about 40% of the total acid sites for metal modified SAPO-34 molecular sieves prepared by impregnation, which will be propitious to the formation of poly-cyclic aromatic hydrocarbons due to the formation of a large number of T-OH (T=Si, P, Al) groups [13]. Relatively, Ni-SAPO-34-8h has the maximum number of medium-strong acid sites, indicating that the N atoms in the template have a suitable induction force for Ni ions.

2. MTO Reaction Performance

The catalytic performance of SAPO-34 molecular sieves in MTO reaction was investigated under reaction condition that the feed WHSV was 2.0 h^{-1} and the amount of catalyst was 0.5 g at 400 °C and at atmospheric pressure. As can be seen from Table 5, the selectivity of light olefins and the catalytic lifetime prepared by template-assisted method are all greater than that of SAPO-34 molecular sieves prepared by impregnation. Zn-SAPO-34-8h catalyst exhibits a relatively short catalytic life and low selectivity of light olefins in comparison with Co-SAPO-34-8h and Ni-SAPO-34-8h, which is attributed to the substantial decrease of total acid sites providing fewer active sites to catalyze the MTO reaction. Metal modified SAPO-34 molecular sieves synthesized by impregnation are prone to the formation of ethylene, which is mainly because the pores of the molecular sieves are blocked by introduction of metal ions, thereby further enhancing the diffusion limited of products [4,36].

The selectivity of products and methanol conversion as a function of time in the stream under optimal conditions of the reaction temperature at 400 °C, WHSV of 2.0 h^{-1} and amount of catalyst of 0.5 g are presented in Fig. 8. In the beginning, all SAPO-34 molecular sieves exhibit a high methanol conversion approaching to 100%, then the methanol conversion decreases little by little due to the coverage of acid sites of the SAPO-34 molecular sieves, as shown in Fig. 8(a)-(g). At the same time, the selectivity of light olefins increases with the extended time on stream. The selectivity of methane also gradually increases with increasing of reaction time because of the gradual deactivation of the SAPO-34 [13]. The selectivity of ethylene increases and the selectivity of propylene and butylene decreases gradually during the reaction period, which can be ascribed to the fact that the small amount of coke can reduce the pore of the SAPO-34 molecular sieves. The effective diffusion coefficient decreases in the following order: butylene>propylene>methanol>ethylene>methane in SAPO-34 molecular sieves [36, 37]. This means that products or reactants with a small diffusion

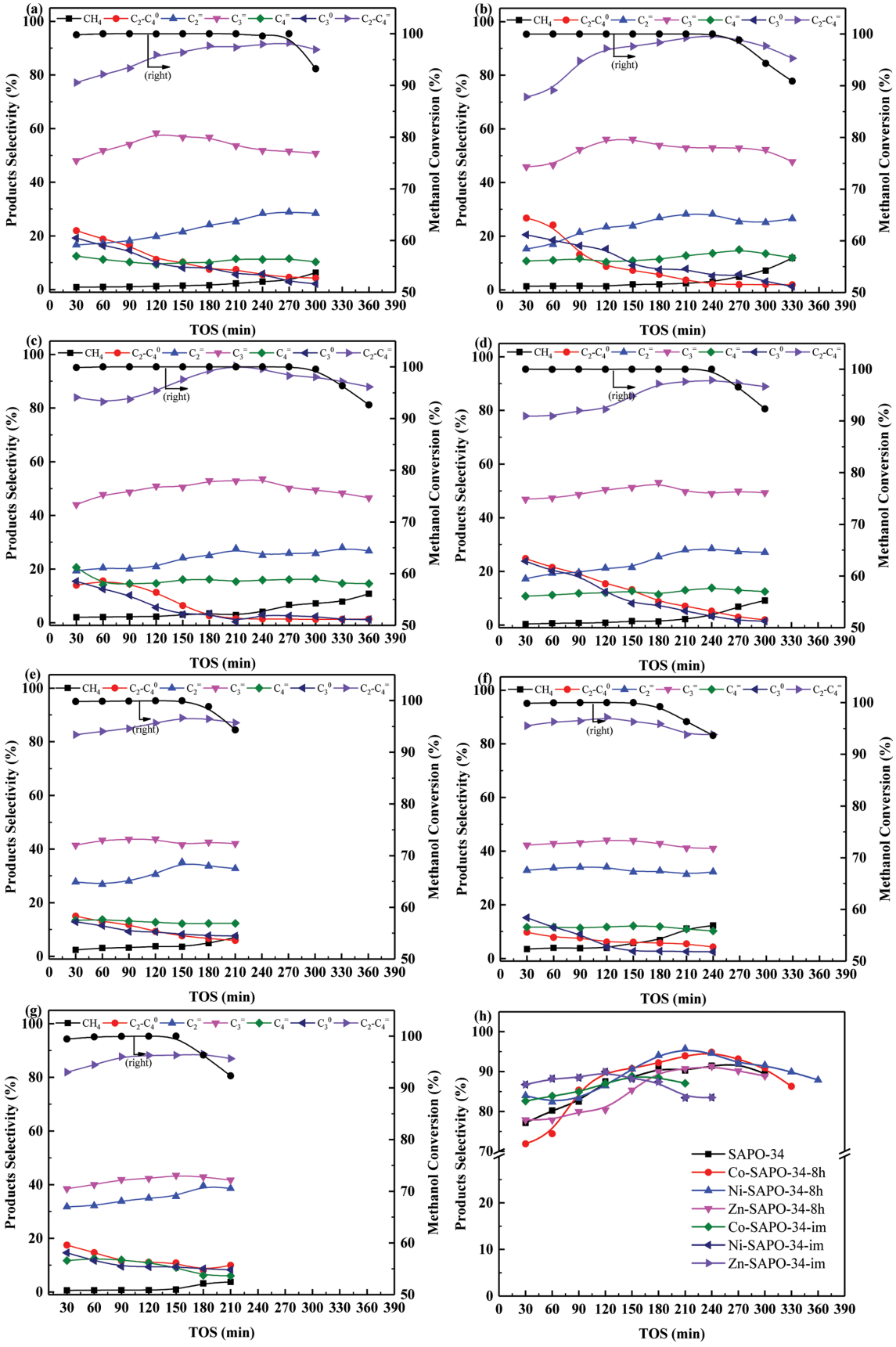


Fig. 8. Products distribution curves of (a): SAPO-34, (b): Co-SAPO-34-8h, (c): Ni-SAPO-34-8h, (d): Zn-SAPO-34-8h, (e): Co-SAPO-34-im, (f): Ni-SAPO-34-im, (g): Zn-SAPO-34-im and (h): the selectivity of light olefins variation with time on stream.

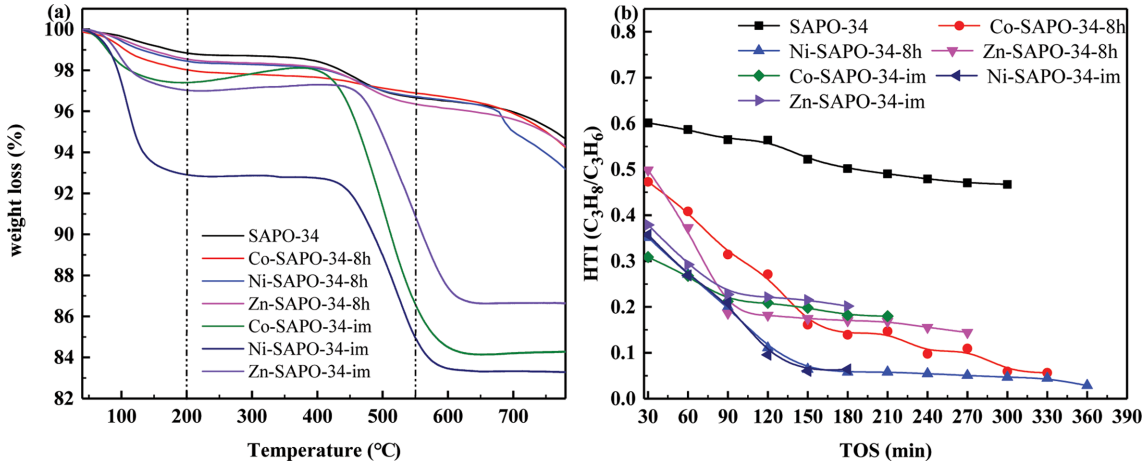


Fig. 9. Thermo-gravimetric curves of (a) catalysts and (b) hydrogen transfer index.

coefficient can easily get into and out of SAPO-34 molecular sieves [38]. As shown in Fig. 8(h), metal modified SAPO-34 molecular sieves prepared by template-assisted method have a relatively higher selectivity to light olefins in comparison with that of metal modified SAPO-34 molecular sieves prepared by impregnation.

The TG profiles of the catalysts after reaction of 6.0 h are shown in Fig. 9(a). The results evidently exhibit the three weight loss steps and similar patterns of weight loss in temperature range of 30 °C-800 °C. The first weight loss step at temperature less than 200 °C is regarded as the desorption of physical water [1]. The second weight loss stage in the temperature range of 200 °C to 550 °C matches the combustion decomposition of the residual template. The third weight loss stage at temperature exceeding 550 °C is attributed to the removal of organics deposited in the internal channels and cages of the SAPO-34 molecular sieve [25]. The deposition rate of carbon is documented in Table 4. It can be seen clearly that the carbon deposition rate of Co-SAPO-34-8h, Ni-SAPO-34-8h and Zn-SAPO-34-8h molecular sieves slightly reduces in comparison with SAPO-34, indicating that introduction of Co, Ni and Zn is beneficial to retard the formation of carbon sediment. In contrast, the carbon deposition rate of Co-SAPO-34-im, Ni-SAPO-34-im and Zn-SAPO-34-im evidently increases, which is ascribed to the formation of excessive T-OH (T=Si, P, Al) groups. The T-OH (T=Si, P, Al) groups can result in the formation of polycyclic aromatic hydrocarbons [39].

The selectivity of light olefins is associated with the number of acid sites and secondary reaction, and the catalysts with temperate acidity are prone to product propylene [2]. Hence, the hydrogen transfer index (HTI, the ratio of C_3H_8/C_3H_6) was employed to evaluate the secondary hydrogen transfer level of olefins [40]. As shown in Fig. 9(b), the HTI value of all metal modified SAPO-34 molecular sieves is lower than that of SAPO-34 molecular sieves, suggesting the secondary hydrogen can be restricted by the introduction of metal species. The initial HTI value of metal modified SAPO-34 molecular sieves prepared by impregnation is lower than that of metal modified SAPO-34 molecular sieves prepared by template-assisted due to that the decrease of acid sites has a negative effect on secondary reactions, but it also implies the decrease of active sites [2]. Moreover, the staple aromatic compounds formed are the monocyclic and bi-cyclic aromatics at initial stage, which may occupy the acid sites and inhibit the capacity of secondary hydrogen transfer [36]. To sum up, metal modified SAPO-34 molecular sieves prepared by template-assisted can enhance the selectivity of light olefins. Ni-SAPO-34-8h has the highest selectivity of light olefins, exhibiting the best MTO performance in this work.

DISCUSSION

It is widely recognized that the primary conversion of methanol strongly relies on the structural integrity of the catalyst [41,42]. The results of XRD and SEM demonstrate that all the catalysts exhibit an integrated CHA structure, which provides a fundamental condition for methanol to light olefins reaction. The relationship between metal ions and template is explored by XPS technique. The N atoms of TEAOH for as-made SAPO-34 show different forces to the Co, Ni and Zn ions and provide the limited anchoring sites; thus the forces between N in the TEAOH and metal ions can control the content of the Co, Ni and Zn ions.

The MTO reaction is a sophisticated acid-catalyzed reaction network which heavily depends on properties of acids [4]. Thus, the acidity of the molecular sieves has significant impact on methanol conversion and product distribution. The weak acid sites provided by many T-OH (T=Si, Al, P) are instrumental in the formation of polycyclic aromatic hydrocarbons, the strong acid sites supplied by Brønsted acid sites cause the part of side reaction including the hydrogen transfer and oligomerization reactions that consume alkenes [43]. Metal modified SAPO-34 molecular sieves prepared by template-assisted method possess a sufficient number of strong acid sites in contrast with metal modified SAPO-34 molecular sieves prepared by impregnation, which further create the outstanding ambience for the productivity of light olefins. Meanwhile, metal modified SAPO-34 molecular sieve with the large surface area prepared by template-assisted method can also supply sufficient quantity of active sites for MTO reaction (Table 3). According to test results (Table 5), metal modified SAPO-34 molecular sieves prepared by template-assisted method improve the selectivity to

light olefins and exhibit an excellent selectivity for propylene. In a word, enhanced selectivity to propylene is observed over SAPO-34 catalysts with metal modification, and the improved catalytic performance is usually attributed to the optimization of acidity [22].

For MTO reaction, hydrocarbon pool mechanism (HCP), which reflects a dynamic change where hydrocarbon pool species is continually adding methanol and splitting off ethylene and propylene. The hydrocarbon pool species can advance methanol conversion and improve the selectivity of propylene at initial reaction stage [2,44-47]. Recently, Olsbye group proposed a more complex dual-cycle mechanism (i.e., an olefins-based cycle and aromatics-based cycle), which proved that the olefin methylation and cracking based on olefin-based cycle is the main route for the production of propylene [37,48]. In addition, some groups verified that the olefin-based cycle at the initial stage of the MTO conversion is the master reaction mechanism, especially on the molecular sieves with weak Brønsted acid sites [26,49]. Direct cracking of hexene over SAPO-34 molecular sieves can promote the productivity of propylene [50]. In the process of cracking of hexene, the 1-hexene with smaller kinetic diameter easily accesses the channels of SAPO-34 molecular sieves, but the iso-hexene isomer is difficult to diffuse into the interior of SAPO-34 molecular sieves due to its microporosity. However, SAPO-34 molecular sieves with mesopore structure can enhance the diffusion of the iso-hexene isomers; thus the productivity of propylene is further improved based on direct cracking route. Besides, Kim and co-worker found that the proper number of the active acid sites via controlling the size (about 3.3 μm) and acidity of SAPO-34 can transform ethylene into propylene based on the oligomerization-cracking reaction [51].

CONCLUSIONS

Co-SAPO-34-8h, Ni-SAPO-34-8h and Zn-SAPO-34-8h molecular sieves were successfully prepared by template-assisted approach without template pre-removal. The metal modified SAPO-34 molecular sieves prepared by template-assisted method maintained an excellent integrity, higher surface area, bigger pore volume and better dispersion of metals. The nitrogen atoms of the template showed different forces for Co^{2+}, Ni^{2+} and Zn^{2+}, which caused the different metal content. Compared to SAPO-34 molecular sieves, the strength and the number of acid sites in Co-SAPO-34-8h, Ni-SAPO-34-8h and Zn-SAPO-34-8h molecular sieves were decreased and Ni-SAPO-34-8h possessed the greater amount of medium-strong acid sites. Metal modified SAPO-34 molecular sieves prepared by template-assisted method were beneficial to the decrease of carbon deposit. Ni-SAPO-34-8h exhibited outstanding selectivity to light olefins.

ACKNOWLEDGEMENTS

This work was financially supported by the National Natural Science Foundation of China (No. 2186503).

CONFLICTS OF INTEREST

There are no conflicts of interest to declare.

REFERENCES

1. W. L. Dai, X. Wang, G. J. Wu, N. J. Guan, M. Hunger and L. D. Li, *ACS Catal.*, **1**, 292 (2011).
2. X. Q. Hu, L. Yuan, S. M. Cheng, J. L. Luo, H. P. Sun, S. P. Li, L. Li and C. Wang, *Catal. Commun.*, **123**, 38 (2019).
3. S. U. Lee, Y. J. Lee, J. R. Kim, K. E. Jeong and S. Y. Jeong, *J. Ind. Eng. Chem.*, **79**, 443 (2019).
4. H. W. Huang, H. R. Wang, H. Zhu, S. H. Zhang, Q. Zhang and C. Y. Li, *Catal. Sci. Technol.*, **9**, 2203 (2019).
5. M. Yang, D. Fan, Y. X. Wei, P. Tian and Z. M. Liu, *Adv. Mater.*, **31**, 1902181(2019).
6. D. Y. Xi, Q. M. Sun, X. X. Chen, N. Wang and J. H. Yu, *Chem. Commun.*, **51**, 11987 (2015).
7. J. W. Zheng, J. J. Ding, D. L. Jin, G. H. Ye, K. K. Zhu, X. G. Zhou, W. M. Yang and W. K. Yuan, *Chem. Commun.*, **53**, 6132 (2017).
8. J. W. Zhong, J. F. Han, Y. X. Wei, S. T. Xu, T. T. Sun, X. W. Guo, C. S. Song and Z. M. Liu, *Chin. J. Catal.*, **39**, 1821 (2018).
9. Q. M. Sun, Z. K. Xie and J. H. Yu, *Natl. Sci. Rev.*, **5**, 542 (2018).
10. J. W. Zhong, J. F. Han, Y. X. Wei, P. Tian, X. W. Guo, C. S. Song and Z. M. Liu, *Catal. Sci. Technol.*, **7**, 4905 (2017).
11. D. Chen, K. Moljord and A. Holmen, *Micropor. Mesopor. Mater.*, **164**, 239 (2012).
12. W. L. Dai, G. J. Wu, L. D. Li, N. J. Guan and M. Hunger, *ACS Catal.*, **3**, 588 (2013).
13. N. Nishiyama, M. Kawaguchi, Y. Hirota, D. V. Vu, Y. Egashira and K. Ueyama, *Appl. Catal. A*, **362**, 193 (2009).
14. C. Wang, M. Yang, P. Tian, S. T. Xu, Y. Yang, D. H. Wang, Y. Y. Yuan and Z. M. Liu, *J. Mater. Chem.*, **3**, 5608 (2015).
15. Q. M. Sun, N. G. Wang, Q. X. Guo, X. Chen and J. H. Yu, *J. Mater. Chem.*, **3**, 19783 (2015).
16. E. Aghaei, M. Haghighi, Z. Pazhohniya and S. Aghamohammadi, *Micropor. Mesopor. Mater.*, **226**, 331 (2016).
17. L. Xu, Z. M. Liu, A. P. Du, Y. X. Wei and Z. G. Sun, *Stud. Surf. Sci. Catal.*, **147**, 445 (2004).
18. S. Aghamohammadi, M. Haghighi and M. Charghand, *Mater. Res. Bull.*, **50**, 462 (2014).
19. H. J. Chae, S. S. Park, Y. H. Shin and M. B. Park, *Micropor. Mesopor. Mater.*, **259**, 60 (2018).
20. Y. W. Liu, Z. Li, Q. Y. Yu, Y. F. Chen, Z. W. Chai, G. F. Zhao, S. J. Liu, W. C. Cheong, Y. Pan, Q. H. Zhang, L. Gu, L. R. Zheng, Y. Wang, Y. Lu, D. S. Wang, C. Chen, Q. Peng, Y. Q. Liu, L. M. Liu, J. S. Chen and Y. D. Li, *J. Am. Chem. Soc.*, **141**, 9305 (2019).
21. A. Turrina, E. C. V. Eschenroeder, B. E. Bode, J. E. Collier, D. C. Apperley, P. A. Cox, J. L. Casci and P. C. Wright, *Micropor. Mesopor. Mater.*, **215**, 154 (2015).
22. J. W. Zhong, J. F. Han, Y. X. Wei, S. T. Xu, T. T. Sun, X. W. Guo, C. S. Song and Z. M. Liu, *J. Energy Chem.*, **32**, 174 (2019).
23. X. Xiang, M. Yang, B. B. Gao, Y. Y. Qiao, P. Tian, S. T. Xu and Z. M. Liu, *RSC Adv.*, **12544**, 6 (2016).
24. Z. M. Liu, L. X. Yang, L. Xu, C. L. Sun and Y. J. Xiong, US Patent, 6,448,191 (2012).
25. H. F. Tian, J. H. Yao, F. Zha, L. Yao and Y. Chang, *Appl. Clay Sci.*, **184**, 105392 (2020).
26. W. L. Dai, C. M. Wang, M. Dyballa, G. J. Wu, N. J. Guan, L. D. Li, Z. K. Xie and M. Hunger, *ACS Catal.*, **5**, 317 (2015).

27. X. Wang, W. X. Chen, L. Zhang, T. Yao, W. Liu, Y. Lin, H. X. Ju, J. C. Dong, L. R. Zheng, W. S. Yan, X. S. Zheng, Z. J. Li, X. Q. Wang, J. Yang, D. S. He, Y. Wang, Z. X. Deng, Y. Wu and Y. D. Li, *J. Am. Chem. Soc.*, **139**, 9419 (2017).
28. W. Shi, B. S. Zhang, Y. M. Lin, Q. Wang, Q. Zhang and D. S. Su, *ACS Catal.*, **6**, 7844 (2016).
29. N. H. N. Kamarudin, A. A. Jalil, S. R. Triwahyono, R. Mukti, M. A. A. Aziz, H. D. Setiabudi, M. N. M. Muhid and H. Hamdan, *Appl. Catal. A*, **431**, 104 (2012).
30. S. Tamiyakul, W. Ubolcharoen, D. N. Tungasmita and S. Jongpatiwut, *Catal. Today*, **256**, 325 (2015).
31. X. Y. Li, J. X. Yang, R. Xu, L. F. Lu, F. G. Kong, M. Liang, L. J. Jiang, S. X. Nie and C. L. Si, *Ind. Crops. Prod.*, **135**, 196 (2019).
32. H. Yang, X. H. Liu, G. Z. Lu and Y. Q. Wang, *Micropor. Mesopor. Mater.*, **225**, 144 (2015).
33. A. K. Singh, R. Yadav and A. Sakthivel, *Micropor. Mesopor. Mater.*, **181**, 166 (2013).
34. M. Salmasi, S. Fatemi and A. T. Najafabadi, *J. Ind. Eng. Chem.*, **17**, 755 (2011).
35. T. Alvaromunoz, C. Marquezalvarez and E. Sastre, *Catal. Today*, **179**, 27 (2012).
36. M. B. Gao, H. Li, M. Yang, J. B. Zhou, X. S. Yuan, P. Tian, M. Ye and Z. M. Liu, *Chem. Eng. J.*, **337**, 119668 (2019).
37. P. F. Wang, F. Zha, L. Yao and Y. Chang, *Appl. Clay. Sci.*, **163**, 249 (2018).
38. S. T. Yang, J. Y. Kim, H. J. Chae, M. Kim, S. Y. Jeong and W. S. Ahn, *Mater. Res. Bull.*, **47**, 3888 (2012).
39. H. A. Sali, O. Muraza, B. Abussaud, T. K. Al-Shammari and T. Yokoi, *Ind. Eng. Chem. Res.*, **57**, 6639 (2018).
40. D. Z. Zhang, Y. X. Wei, L. Xu, F. X. Chang, Z. Y. Liu, S. H. Meng, B. L. Su and Z. M. Liu, *Micropor. Mesopor. Mater.*, **116**, 684 (2008).
41. M. Firoozi, M. Baghalha and M. Asadi, *Catal. Commun.*, **10**, 1582 (2009).
42. I. Othman, R. M. Mohamed, I. A. Ibrahim and M. M. Mohamed, *Appl. Catal. A*, **299**, 95 (2006).
43. D. Chen, K. Moljord and A. Holme, *Micropor. Mesopor. Mater.*, **164**, 239 (2012).
44. I. U. Din, M. S. Shaharun, A. Naeem, S. Tasleem and M. R. Johan, *Chem. Eng. J.*, **334**, 619 (2018).
45. B. Q. Jing and J. F. Li, *Chemistry Select*, **4**, 7634 (2019).
46. W. G. Song, J. F. Haw, J. B. Nicholas and C. S. Heneghan, *J. Am. Chem. Soc.*, **122**, 10726 (2000).
47. J. F. Haw and D. M. Marcus, *Top Catal.*, **34**, 41 (2005).
48. U. Olsbye, S. Svelle, M. Bjorgen, P. Beato, T. V. W. Janssens, F. S. Bordiga and K. P. Lillerud, *Angew. Chem.*, **51**, 5810 (2012).
49. W. L. Dai, G. Cao, L. Yang, G. J. Wu, M. Dyballa, M. Hunger, N. J. Guan and L. D. Li, *Catal. Sci. Technol.*, **7**, 607 (2017).
50. Z. Nawaz, X. P. Tang, J. Zhu, F. Wei and S. Naveed, *Chin. J. Catal.*, **30**, 1049 (2009).
51. H. J. Kim, J. W. Kim, N. Kim, T. W. Kim, S. H. Jhung and C. U. Kim, *Mol. Catal.*, **438**, 86 (2017).